A fast online frequency adaptation mechanism for CPG-based robot motion control

Mathias Thor[1] and Poramate Manoonpong[1]

***Abstract*—In this letter, we present an online learning mechanism called the Dual Integral Learner for fast frequency adaptation in neural Central Pattern Generator (CPG) based locomotion control of a hexapod robot. The mechanism works by modulating the CPG frequency through synaptic plasticity of the neural CPG network. The modulation is based on tracking error feedback between the CPG output and joint angle sensory feedback of the hexapod robot. As a result, the mechanism will always try to match the CPG frequency to the walking performance of the robot, thereby ensuring that the entire generated trajectory can be followed with low tracking error. Real robot experiments show that our mechanism can automatically generate a proper walking frequency for energy-efficient locomotion with respect to the robot body as well as being able to quickly adapt the frequency online within a few seconds to deal with external perturbations such as leg blocking and a variation in electrical power. These important features will allow a hexapod robot to be more robust and also extend its operating time. Finally, the generality of the mechanism is shown by successfully applying it to a compliant robotic manipulator arm called GummiArm.**

***Index Terms*—Legged Robots, Neurorobotics, Robust/Adaptive Control of Robotic Systems**

I. INTRODUCTION

LOCOMOTION generation in hexapod robots has been widely studied [1], [2], [3]. Compared with bipedal robots, hexapod robots have better flexibility and stability, making them more suitable for complex environments [4]. In term of adaptation, Cully et al. [5] showed how a repertoire of locomotion behaviors could be used to make the system fault tolerant. When the hexapod robot is damaged (e.g., broken or missing legs), the controller starts to search for new locomotion behaviors to cope with the new state of the robot using a trial-and-error learning algorithm. This adaptation process requires a few minutes to obtain an appropriate new walking behavior. Steingrube et al. [6] demonstrated environmental-dependent adaptation of a hexapod robot by using chaos control with a modified Widrow-Hoff learning mechanism. While the chaos control can generate various gaits, the learning mechanism allows the robot to select a proper gait for walking up a slope. This learning scheme needs several minutes to obtain the upslope gait. Schneider et al. [7] showed an adaptive bio-inspired control approach, combining Walknet [8] with higher level control and planning for adaptive interlimb coordination of the hexapod robot HECTOR. Using this approach, various behaviors (e.g., gap crossing, obstacle crossing, and global planning) can be generated to adapt to complex environments. Owaki et al. [9] introduced another method for hexapedal interlimb coordination and adaptation called the Tegotae-based approach. Tegotae is a Japanese concept for describing how well a perceived reaction matches an intention. The approach works by increasing the Tegotae for each limb in a robot, i.e., the difference between the intention of the controller and the reaction from the environment. Through this approach, a hexapod robot can perform self-organized locomotion and adapt to changes in weight distribution as well as leg amputation.

Different learning and adaptation mechanisms have been developed for hexapod robots such that they can not only walk but also show adaptation. The adaptation can usually deal with leg damage or amputation, weight distribution, and changes in the environment. Achieving fast online adaptation within a few seconds for energy-efficient locomotion, damage prevention, and even dealing with a variation in electrical power, has still not been sufficiently addressed.

From this perspective, this letter proposes an online learning mechanism that can automatically generate a proper walking frequency for energy-efficient hexapod locomotion as well as quickly adapt online to prevent damage and deal with a variation of electrical power. It does so by modulating the CPG frequency through synaptic plasticity of a neural CPG network. The modulation is based on tracking error feedback between the CPG output and a joint angle signal of a hexapod robot. In principle, it adapts to the highest CPG frequency at which the robotic system can follow the entire generated CPG trajectory with low tracking error. By doing so, it ensures that the CPG frequency matches the performance of the robot, thereby utilizing its full potential.

The consequences of controlling a hexapod robot at a frequency that cannot be followed include loss of precision, unwanted movement, energy-inefficient locomotion, and in the worst-case motor collapse. The tracking error may also impact the performance of the control system since the desired trajectory is not followed as expected. This is especially critical in

Manuscript received: February, 20, 2019; Revised May, 21, 2019; Accepted June, 22, 2019.

This paper was recommended for publication by Editor N. Tsagarakis upon evaluation of the Associate Editor and Reviewers' comments. This work was supported by FETPROACT (grant no. 732266 (Plan4Act)), the Thousand Talents program of China, and the startup grant from VISTEC.

[1]M. Thor and P. Manoonpong are with the Embodied AI & Neurorobotics Lab, Centre for BioRobotics, The Mærsk Mc-Kinney Møller Institute, The University of Southern Denmark, Odense M, Denmark. P. Manoonpong is also with the College of Mechanical and Electrical Engineering, Nanjing University of Aeronautics and Astronautics, China and School of Information Science & Technology, Vidyasirimedhi Institute of Science & Technology, Thailand. mathias@mmmi.sdu.dk & poma@nuaa.edu.cn

This paper has supplementary downloadable material available at http://ieeexplore.ieee.org, provided by the authors. This includes five multimedia .mp4 format video clips, which show the five experiments presented in this letter. This material is 28.8 MB in size.

Digital Object Identifier (DOI): see top of this page.

research concerning trajectory optimization for efficient robot locomotion or manipulation behaviors.

The learning mechanism developed to reduce the tracking error is called the Dual Integral Learner (DIL), which is based on the Dual Learner (DL) by Smith et al. [10]. This mechanism uses simple gain and integrator terms, directly relating to error reduction. This is an advantage when compared to state-of-the-art online frequency learning mechanisms like adaptive frequency oscillators (AFOs) [11] and frequency adaptation through fast dynamical coupling (AFDC) [12] since these rely on a desired correlation or phase shift between the CPG output and sensory feedback. Such a phase shift is easy to determine for simple systems (e.g., a mathematical pendulum). However, when applying such mechanisms to control complex systems (e.g., a walking robot) trial and error experiments are required to determine the phase shift. Furthermore, in the case of legged robots, a phase shift that guarantees near optimal locomotion is hard to find [13]. Hence, the motivation for using error-based learning over correlation-based learning is its simplicity and excellent performance in terms of fast and versatile adaptation with low tracking error to deal with different conditions. The DIL can, in this way, be seen as a proposed improvement to our state-of-the-art correlation-based learning mechanism AFDC.

Therefore, the main contributions of this letter are: 1) to describe the novel DIL mechanism used to quickly reduce an error (sections II-A); and 2) to demonstrate how the DIL can be integrated with neural CPG-based control to reduce the tracking error of the joints in a hexapod robot (Sect. III). Finally, the mechanism will be evaluated against the state-of-the-art learning mechanism AFDC [12] (Sect. III-B) and also applied to a compliant robotic manipulator to determine the strengths and generality of our approach (Sects. IV and V). To this end, the proposed approach can drive a hexapod robot for energy-efficient locomotion and give fast online adaptation within a few seconds to prevent leg damage as well as being able to deal with a variation of electrical power. These important features will allow a hexapod robot to be more robust and extend its operating time.

II. Frequency adaptation mechanisms

A. Dual Integral Learner

The DIL, used for error reduction, is based on the DL presented by Smith et al. [10]. One of the key aspects of this learner is that it uses fast and slow learners in parallel as shown in Fig. 1. Each leaner receives the same error and incorporates a proportion of it into their current estimate of the perturbation [14]. This is shown by the rules in (1):

$$\begin{aligned} x_f(n) &= A_f \cdot x_f(n-1) + B_f \cdot e(n) \\ x_s(n) &= A_s \cdot x_s(n-1) + B_s \cdot e(n) \\ x(n) &= x_s(n) + x_f(n) \\ e(n) &= f(n) - x(n) \end{aligned} \tag{1}$$

where $x_f(n)$ is the output of the fast learner, $x_s(n)$ is the output of the slow learner, $x(n)$ is the combination of the two outputs, $e(n)$ is the error or difference between the output $x(n)$ and a setpoint $f(n)$, B_f and B_s are learning rates, and A_f and A_s are retention factors. The parameter selection is under the constraint that $B_f > B_s$ and $A_f < A_s$. The fast learner consequently learns faster as indicated by a higher learning rate but also forgets more rapidly as indicated by a lower retention factor.

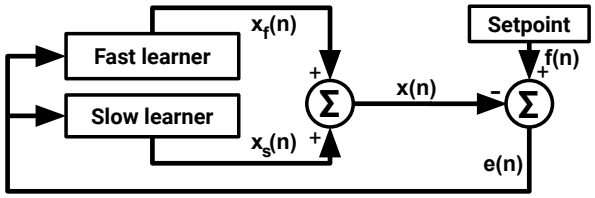

Fig. 1: Block diagram of the DIL. The system output ($x(n)$) is the sum of the outputs from the fast ($x_f(n)$) and slow learners ($x_s(n)$). The error ($e(n)$) is the difference between the system output and the setpoint ($f(n)$).

The main advantages of this approach are error reduction, saving in relearning, and spontaneous recovery of previously learned memories (for a detailed explanation see [14]). However, the DL suffers from steady-state errors since it only includes learning rates and retention factors.

To address this issue, we propose the DIL that include additional integrator components in the two learners. This is shown with the rules in (2):

$$\begin{aligned} x_f(n) &= A_f \cdot x_f(n-1) + B_f \cdot e(n) + C_f \cdot \textstyle\int e(n) \\ x_s(n) &= A_s \cdot x_s(n-1) + B_s \cdot e(n) + C_s \cdot \textstyle\int e(n) \\ x(n) &= x_s(n) + x_f(n) \\ e(n) &= f(n) - x(n) \end{aligned} \tag{2}$$

where the new parameters C_f and C_s are the integrator components, accumulating the error over time to make the learning process correct it. Note that the new parameters are under the constraints that $C_f > C_s$.

Fig. 2 shows a learning simulation in the DL and DIL when exposed to an arbitrary square wave setpoint input alternating bet ween 0, +1, -1, and +1 again (cf. Fig. 1). It can be seen that both the DL and DIL show savings in relearning and that they are able to spontaneously recover to +1 again when the setpoint is briefly set to -1. The simulation also shows that the use of the integrator components enables the DIL to remove the error (i.e., the difference between the setpoint and learner output) which the DL is not fully able to.

III. Neural CPG-based Control

In the experiments presented in Sect. IV, the Modular Robot Framework (MORF) [15] is used as a testbed. MORF can be configured as either a mammal or an insect with a different number of legs. For the purpose of this study an insect configuration with six legs, i.e., a hexapod configuration (shown in Fig. 3), will be used.

In order to control MORF, a neural CPG-based controller that makes it walk with a tripod gait has been developed [6]. The main component of the controller is the neural SO(2) oscillator [16] (acting as a CPG, see Fig. 4). The SO(2)-based CPG is a versatile recurrent neural network consisting

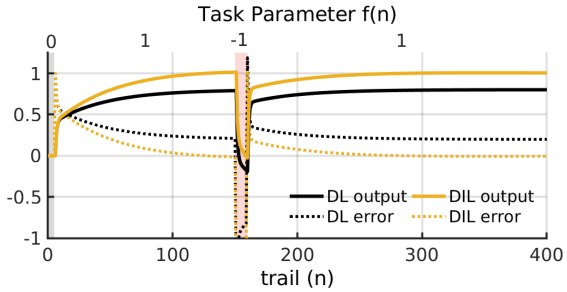

Fig. 2: Simulation of learning in the DL (shown in black) and DIL (shown in orange) when exposed to a square wave setpoint input. The initial setpoint is 0 in the gray zone, +1 in the white zones, and -1 in the red zone. The error is given as the difference between the setpoint and learner output. Unlike the DIL, the DL is not able to fully remove the error.

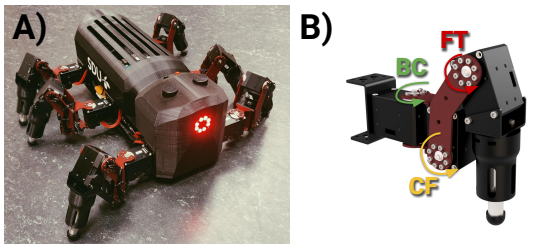

Fig. 3: A) MORF in a hexapod configuration [15]. B) Each leg consists of three joints; the body-coxa (BC) joint, the coxa-femur (CF) joint, and the femur-tibia (FT) joint.

of two fully-connected standard additive time-discrete neurons H_0 and H_1, both using a sigmoid transfer function. The SO(2) oscillator can exhibit various dynamical behaviors (e.g., periodic patterns, chaotic patterns, and hysteresis effects [6]) by changing its synaptic weights. These dynamical behaviors of the network can later be exploited for complex locomotion behaviors. However, the DIL can also be integrated into other CPG models (e.g., the Van der Pol oscillator [17], Hopf oscillator, or Rayleigh oscillator [18]) since it only requires a way to vary the frequency of the CPG.

The outputs of the two neurons in the SO(2) oscillator are given by (3):

$$o_i(t+1) = tanh\left(\sum_{j=0}^{N} w_{ij}(t)o_j(t)\right), \quad i = 0, ..., N \qquad (3)$$

where o_i is the output from neuron i, N is the number of neurons, and w_{ij} is the synaptic weight from neuron i to j. The two neurons both produce a sinusoidal output with a phase shift of $\pi/2$.

As proven by Pasemann et al. [16] the network produces a quasi-periodic output when the weights are chosen, according to (4):

$$\begin{pmatrix} w_{00}(t) & w_{01}(t) \\ w_{10}(t) & w_{11}(t) \end{pmatrix} = \alpha \cdot \begin{pmatrix} \cos\ \varphi(t) & \sin\varphi(t) \\ -\sin\ \varphi(t) & \cos\varphi(t) \end{pmatrix} \qquad (4)$$

with $0 < \varphi(t) < \pi$ as the frequency determining parameter. Parameter α determines the amplitude and the nonlinearity

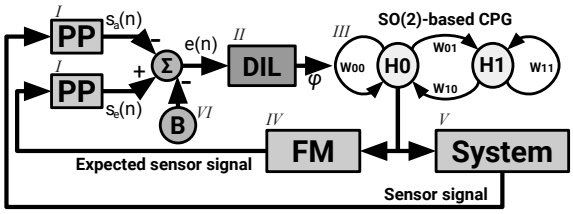

Fig. 4: Neural CPG-based control network, combining the SO(2) oscillator with the DIL. *I)* The post-processing (PP) is responsible for calculating the amplitude from the incoming signal and filtering it using a digital low-pass single-pole IIR filter. *II*) The DIL mechanism. *III)* The neural SO(2) oscillator based CPG model. *IV)* The forward model (FM) for translating the CPG outputs into expected sensor signals. *V)* The robotic system (i.e., the MORF hexapod robot) controlled by the CPG. *VI)* The bias enabling the mechanism to increase the frequency in the case of no tracking error.

of the output oscillations. For this controller, $\alpha = 1.01$ is used to obtain harmonic oscillation and an approximate linear relationship between φ and the intrinsic frequency of the oscillator [12].

The two outputs from the SO(2)-based CPG, having a phase shift of $\pi/2$, are first post-processed and subsequently sent as position commands to the BC and CF joints. The designed intralimb coordination makes the two joints move with a phase shift of $\pi/2$ such that the CF joints move first, followed by the BC joints. This way, the legs will be lifted above the ground by the CF joints before being moved forward by the BC joints and lowered down before moving backward. This is to ensure ground clearance during a swing phase and ground contact during a stance phase. Note that the FT joints are set to fixed positions for simplicity. For interlimb coordination to obtain a tripod gait, we define the coordination by projecting the CPG outputs through inhibitory synaptic weights (-1) to the BC and CF joints of the left middle, right front, and right hind legs and excitatory synaptic weights $(+1)$ to the BC and CF joints of the remaining legs.

A. Neural CPG-based Control with DIL

In order to let the DIL mechanism adapt the frequency of the SO(2) oscillator, we integrate the DIL into the neural control, resulting in the network shown in Fig. 4. Using this network, the DIL will adapt φ (i.e., $\varphi = x(n)$ where φ refers to the synapses of the SO(2) oscillator, see (4)) based on error feedback $e(n)$. The error feedback is given as the tracking error between the amplitudes of the actual joint angle $s_a(n)$ and the expected joint angle $s_e(n)$ (i.e., $e(n) = s_e(n) - s_a(n)$). The expected joint angle is obtained from a forward model (FM) (*IV*) that is modeled as a simple gain. The FM can calculate the expected sensory signals from the control commands given as input to the system. This makes it possible to compare the CPG output (*III*) with the actual joint angle sensory feedback from the walking robot (*V*). Finally, the amplitudes of the signals are calculated using the two post-processing units (PP) (*I*), which also uses digital low-pass single-pole IRR filters, to remove noise. The calculation

of the amplitudes currently exploits that the SO(2) oscillator is producing a waveform output. Note that the DIL can also be used to adapt the amplitude of the CPG. However, in this work, we only focus on frequency adaptation since a change in amplitude also alters the trajectory performed by the robot. This is not desired when also working with trajectory optimization or robotic manipulators where a specific endpoint is required.

If the amplitude of the expected sensory signal is larger than that of the actual sensor signal, then the network will produce a positive tracking error. The DIL will, in this case, decrease φ since the joints cannot follow the desired trajectory as generated by the CPG. However, negative tracking errors can only occur from external forces and not from the CPG output itself. Thus, in order to enable the DIL to increase the frequency in a reliable way, a small bias B (*VI*) is subtracted from the error. In this way, the DIL will get a negative tracking error when the expected and actual amplitudes match and try to increase φ. An example of the DIL adapting the parameter φ (i.e., synaptic plasticity) in the case of both positive and negative tracking errors is shown in Fig. 5. It should be noted that the bias makes the mechanism run with a small constant tracking error, which in this case 0.005 rad. The bias should be set according to the properties of the system it is used on, i.e., some systems allow more tracking error than others. A larger bias means a larger frequency, larger tracking error, and faster adaptation when increasing the frequency. Furthermore, the bias can be completely removed if the frequency is to be continuously varied by an operator or a navigation module. In this way, the DIL only adapts the frequency when it is larger than a certain maximum value defined by the allowed tracking error in the system.

For the experiments presented in Sect. IV, the network in Fig. 4 uses the joint angle sensory feedback from a BC joint of MORF. This is because this joint is responsible for moving the robot forward during the stance phase and thus directly influences the walking speed (i.e., the DIL will control the walking frequency). In all four experiments, the DIL mechanism uses identical learning parameters; $A_f = 0.6$, $A_s = 0.9$, $B_f = 0.8$, $B_s = 0.4$, $C_f = 0.015$, $C_s = 0.005$, and a bias of 0.008 (i.e., seven parameters in total) since that gives the DIL mechanism the ability to adapt the CPG frequency while maintaining a low tracking error. Note that all parameters are empirically chosen.

When using feedback from a single joint the outputs of both the FM and system (see (IV) and (V) in Fig. 4) have a dimension of one. However, the network is scalable, meaning that it can take multiple joint angle values and calculate the average tracking error. It can also be extended by using multiple CPGs such that each leg or joint adapts independently. This extension is useful in decentralized controllers like the one shown in [19] where each leg has its own CPG.

B. Frequency Adaptation through Fast Dynamical Coupling

To compare the performance of the DIL for frequency adaptation of hexapod walking, the AFDC mechanism by Nachstedt et al. [12] is used. AFDC is a state-of-the-art

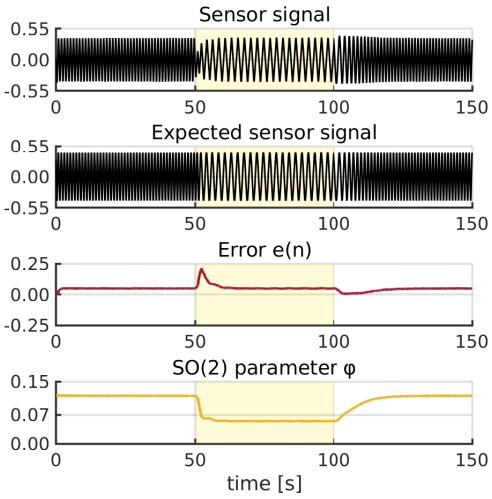

Fig. 5: Simulation of the DIL when used to reduce the tracking error. The yellow zone from 50s to 100s indicates that the maximum frequency of the system is reduced.

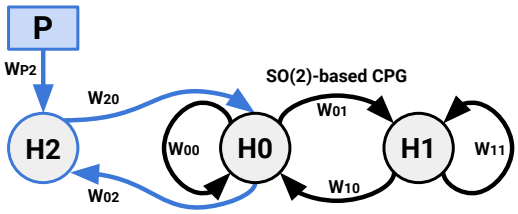

Fig. 6: The AFDC mechanism when used on the neural SO(2) oscillator. The blue parts refer to the AFDC mechanism. It consists of a neuron (H_2), enabling the oscillator to synchronize with the external perturbation P.

frequency adaptation mechanism for CPGs, providing fast and accurate adaptation for a wide range of target frequencies when compared to other classical frequency adaptation mechanisms like AFOs [11]. It does this by dynamically adapting the coupling strength of an external perturbation signal to a CPG. This makes the AFDC engaging in locomotion controllers where a system needs to react quickly to external perturbations.

Fig. 6 shows how the AFDC can be combined with the neural SO(2) oscillator, which is also used in the locomotion controller as explained in the previous section. The dynamic coupling of the AFDC is established using a single extra neuron H_2, connected to the SO(2) oscillator through plastic synapses, W_{20} and W_{02} (blue arrows). The H_2 neuron calculates a filtered version of the external perturbation signal P and receives signals via the synapses W_{02} and W_{P2}. The two synapses are modulated by the rules in (5) [12]:

$$\begin{aligned} W_{02}(t+1) &= W_{02}(t) + (\beta_0 - W_{02}(t) - \kappa \cdot o_2(t) \cdot o_0(t))/\tau \\ W_{P2}(t+1) &= W_{P2}(t) + (\epsilon_0 - W_{P2}(t) - \kappa \cdot P(t) \cdot o_2(t))/\tau \end{aligned} \tag{5}$$

where κ is the correlation learning rate, β and ϵ are adaptive coupling strengths, τ is a time constant, o_0 is the output from neuron H_0, and o_2 is the output from neuron H_2. If a large

difference exists between the intrinsic and target frequencies (i.e., a large phase shift), the coupling strength is increased to speed up the adaptation. On the other hand, if there is a small difference (i.e., a small phase shift), then the coupling strength is decreased to increase the accuracy of the adaptation [12].

Finally, the SO(2) frequency, determined by the parameter φ, is modulated by the rule in (6) [12]:

$$\varphi(t+1) = \varphi(t) + \eta \cdot W_{20}(t) \cdot o_2(t) \cdot W_{01}(t+1) \cdot o_1(t) \quad (6)$$

where η is the learning rate and o_1 is the output from H_1. The modulation of φ influences the synapses of the SO(2) oscillator (w_{00}, w_{01}, w_{10}, and w_{11}, see (4)) in a long-term synaptic plasticity manner. The synaptic plasticity will hereby converge when the phase difference between the CPG output H_0 and external perturbation signal is removed (or when a desired phase shift is obtained).

While the DIL adapts φ based on a tracking error, the AFDC adapts it based on a desired phase shift $\Delta\phi$, between an external perturbation signal and the CPG output. By using the joint angle feedback from a BC joint as the perturbation signal, it is possible to adapt the walking frequency.

Nachstedt et al. [13], described a method for using the AFDC to adapt the frequency of a CPG controlling a six-legged robot. They found that for complex systems, like legged robots, it is not clear which $\Delta\phi$ between a motor command (i.e., CPG output) and joint angle sensory feedback will be optimal. However, by testing various values for $\Delta\phi$, a phase shift of $\Delta\phi = 0.2\pi$ was found to produce the fastest and most energy-efficient locomotion. In the following experimental setups, a phase shift of 0.2π is therefore used when testing the AFDC. The remaining parameters for the AFDC are set according to those specified in [13] with the exception of the learning rate which is set to 8 resulting in much faster adaptation.

IV. Experiments and Discussion

In the following four experiments, the MORF hexapod robot is used to access the performance of the DIL mechanism. MORF weighs 4.2kg and is equipped with Dynamixel XM340-350 smart servos, making it possible to read the power consumption, joint angles, and in extension, to use the locomotion controller presented in Sect. III. The controller is used under the assumption that the periodic shape of the CPG is given according to the neurodynamics of the CPG and that only frequency optimization is required. As described earlier, error feedback to the DIL is defined as the tracking error between the amplitude of one BC joint angle signal and the amplitude of the CPG output driving the joint (efference copy). The BC joint angle signal is likewise used as the perturbation to the AFDC mechanism.

To illustrate the generality of the DIL mechanism a fifth experiment is included where the mechanism is used on a 7 degrees of freedom compliant robotic manipulator arm called GummiArm [20] (see Fig. 7). In contrast to the joints on MORF, some joints on the GummiArm are actuated by three motors. In this setup, one motor acts as a passive stabilizer while the two remaining joints are connected using compliant

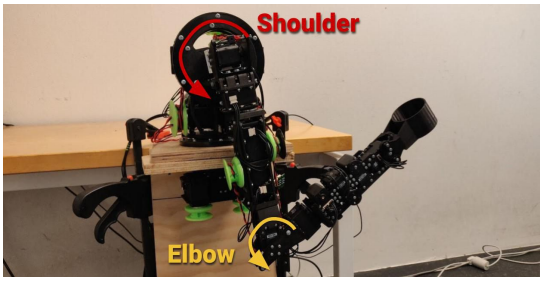

Fig. 7: The GummiArm robot [20]. The neural CPG-based controller actuates the shoulder and elbow joints in order to make the arm perform a sawing-like motion.

tendons. Thus, these two motors work as an antagonist-agonist setup, similar to how the human arm is configured. The GummiArm is equipped with the same neural CPG-based control as used on MORF but this time with interlimb coordination making it move in a sawing-like motion. It should be noted that the controller uses the joint angle sensory feedback from the shoulder joint of the GummiArm and the CPG-based controller only actuate the shoulder and elbow joint (see Fig. 7). This is because this joint is responsible for moving the arm back and forth, thus directly influencing the sawing speed.

A. Adaptation to robot body

The first experiment was to determine whether the DIL mechanism can converge to a certain walking frequency (i.e., finding a proper φ), for various initial internal SO(2) frequencies (i.e., various initial values of φ_0). In the experiment, MORF was placed on a stand such that the legs could swing freely in the air.

Fig. 8 shows that φ was adapted for six different initial frequencies. The walking frequency converged to a mean φ of 0.27 with a standard variance of 0.003. This value leads to adapted SO(2) synaptic weights of $w_{00} = 0.992$, $w_{01} = 0.191$, $w_{10} = -0.191$, and $w_{11} = 0.992$.

To analyze why the DIL adapts the CPG frequency to 0.27, a plot of the tracking error and amplitude of the joint angle sensory feedback against the CPG frequency (φ) is made (see Fig. 9). This shows that the DIL, as expected, adapts the frequency to the point where the amplitude begins to decrease and the tracking error increases above the bias. Thus, the DIL mechanism can adapt the CPG to a specific frequency, matching the body property of the MORF hexapod robot which in this case is $\varphi = 0.27$. In other words, by running MORF with a CPG frequency of 0.27, the desired trajectory is performed with a low tracking error and the full potential of the system is utilized (moving with a high frequency/speed and a large angle). If MORF moves with a faster frequency then the tracking error will increase (thereby, it moves with a smaller joint angle amplitude) and if it moves with a lower frequency then the full potential of the system will not be utilized. This mechanism converges toward different walking frequencies depending on the robot characteristics, e.g., different leg morphologies, body weights, and motor performances (as shown in the next experiment and the experiment with the

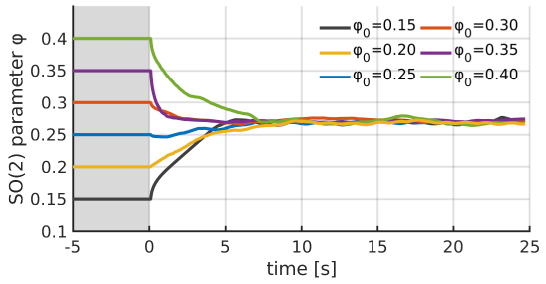

Fig. 8: Adaptation of φ for different initial values φ_0 using the DIL. All of the trials converges to a mean φ of 0.27 with a standard variance of 0.003.

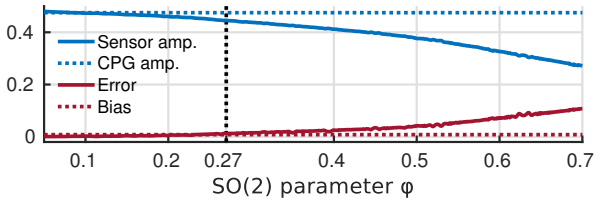

Fig. 9: Plot of the tracking error (red) and sensor amplitude from a BC joint of MORF (blue) against the CPG frequency. The CPG or expected amplitude is shown with a dashed blue line and the bias with a dashed red line.

GummiArm robot). A video of the experiment can be found in the supplementary material (video SM1.mp4).

B. Adaptation to a variation of electrical power

In the second experiment, the DIL was applied to adapt the walking frequency when we abruptly change the voltage or electrical power to the servo motors of MORF during walking. Here, we compared the performance of the DIL with the AFDC. The voltage or stimulus was regulated using an external power supply and changed twice during the experiment. First, it was reduced from 15.5V by 2.7V to 12.8V after 10s of walking and increased back to 15.5V after 30s. This is similar to the discharge cycle of a four-cell LiPo battery if each cell is discharged from 4.2V to 3.5V. The reason for having 15.5V as the maximum voltage and not 16.8V as in a four-cell LiPo battery is that the Dynamixel servos have a maximum input voltage of 16V. When the voltage to the servos is changed, their performance also changes and the frequency adaptation mechanisms need to adapt accordingly. The initial adaptation of the two mechanisms was not included in the experiment.

Fig. 10 shows how the SO(2) parameter φ was adapted in five trials using the AFDC (blue) and DIL (orange) mechanisms. The lines show the mean φ value and mean tracking error while the surrounding transparent area shows the standard variance. The DIL mechanism can reduce the mean tracking error down to 0.008 which is better than the AFDC ($P > 0.999$) which has a mean tracking error of 0.01. It is possible for the DIL to reduce the error even more by choosing a smaller bias. However, this will result in slower adaptation when increasing the frequency. It should be noted that the φ value for the DIL is slightly smaller ($\varphi = 0.25$)

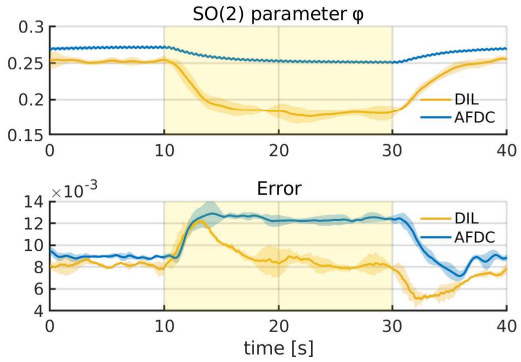

Fig. 10: Adaptation of φ using the DIL (orange) and AFDC (blue) mechanisms. The lines show the mean φ value (upper plot) and mean tracking error (lower plot) while the transparent area surrounding them shows the standard variance. The voltage to the servos is reduced by 2.7V from 10s to 30s (yellow zone). The mean tracking errors for the DIL and AFDC mechanisms are 0.008 and 0.010, respectively. The mean cost of transport for the DIL and AFDC mechanisms are 2.75 and 2.90, respectively.

than the one found in the previous experiment ($\varphi = 0.27$). This is because in the previous experiment MORF was placed on a stand and the legs could move freely whereas here, the legs carried the robot weight during the stance phase.

During the experiment, it was observed that MORF walked less straight with the AFDC than with the DIL (see the supplementary video SM2.mp4). This is due to a consequence of walking with a larger tracking error. Hence, the DIL can maintain straight walking even without additional steering or directional control. The DIL is also useful for a robotic system that is supposed to precisely follow a certain trajectory, as in the domain of trajectory optimization.

Reducing the tracking error also results in a lower cost of transport (CoT), meaning that DIL produces more energy-efficient locomotion. The CoT is calculated as $\frac{P \cdot t}{m \cdot g \cdot d}$, where P is the power consumption of the servos given by $P = V \cdot I$, t is the time in seconds, m is the total mass of MORF in kg, g is the gravity of the earth, and d is the walking distance covered by MORF. In the experimental results shown in Fig. 10, the mean CoT of the DIL and the AFDC are 2.75 and 2.90, respectively. This shows that the DIL leads to more energy-efficient locomotion ($P = 0.880$).

Finally, since the learning parameters of the DIL easily relate to the tracking error reduction, i.e., gain and integrator terms (variables B and C in (2)), the parameters are also easy to tune for other complex systems. In contrast, the AFDC reduces tracking error by tuning a CPG frequency toward a desired phase shift $\Delta\phi$. This phase shift is often chosen to correspond with the system resonance frequency. However, for complex systems, it is not always possible to identify the phase shift; therefore, it has to be found empirically. Furthermore, in the case of legged robots, a phase shift that guarantees next to optimal locomotion is hard to find since there is no intuitive correlation between phase shift, tracking error, and CoT as also pointed out in [13].

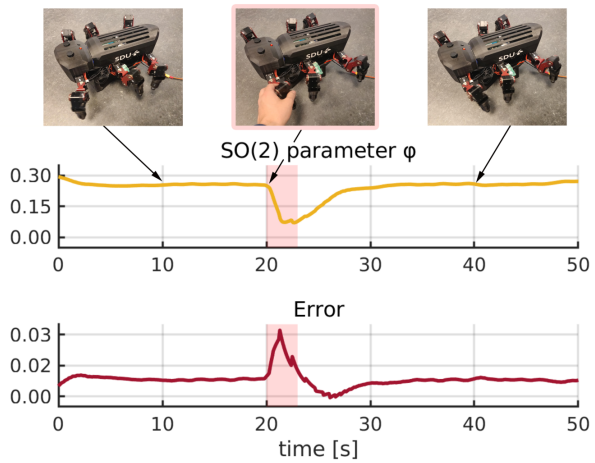

Fig. 11: Adaptation of φ to an external perturbation using the DIL. At 20s (red zone) a leg is shortly blocked by hand. The DIL immediately reduce the CPG frequency to nearly zero in response to the high tracking error, resulting in stopping the leg movement. This way the leg is protected from getting damaged.

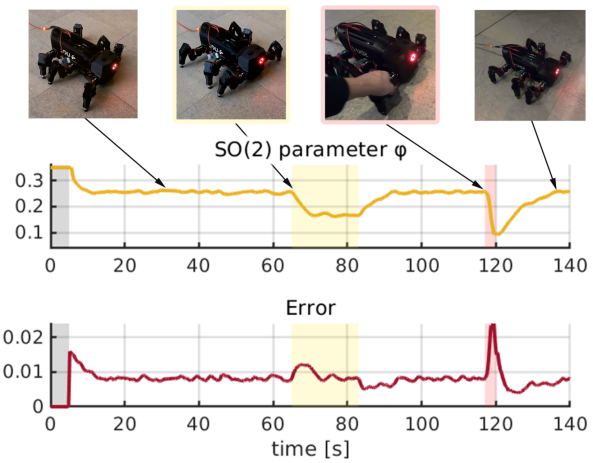

Fig. 12: Adaptation of φ using the DIL. First φ is adapted from an initial value of 0.35, then to a reduction of 2.7V in voltage (yellow zone), and finally to a leg being blocked by hand (red zone). Note that the DIL starts after 5s (gray zone). For the three scenarios, the DIL can adapt φ to obtain a new walking frequency within approximately 5s.

C. Adaptation for damage protection

The third experiment was to determine how the DIL mechanism adapts the walking frequency to an external perturbation. In the experiment, MORF was again placed on a stand to enable the legs to move freely in the air. After 20s a leg was blocked by hand which is equivalent to it getting stuck or hitting an object while walking.

As shown in Fig. 11, the DIL mechanism quickly decreases the walking frequency when the leg is blocked. This behavior can be seen as a self-protection mechanism to prevent damage. A video of the experiment can be found in the supplementary material (video SM3.mp4).

D. Multiple adaptations to unexpected situations during continuous walking

The fourth experiment combined the three adaptation features (adaptation to the body, electrical power variation, and damage protection) during continuous walking. In this continuous walking experiment (shown in Fig. 12), we set an arbitrary initial value of the φ to 0.35 which generates a high walking frequency. The DIL was started after 5s and could quickly adapt to obtain a proper walking frequency in around 5s, allowing MORF to efficiently walk on the floor. At around 60s, MORF experienced a reduction of electrical power. We simulated this by manually reducing the voltage from 15.5V to 12.8V for 20s. In order to maintain its walking performance with a low tracking error, the DIL automatically reduced the walking frequency. At around 83s, MORF received full power again whereby we increased the voltage to 15.5V. This made the DIL increase φ to the value found initially, resulting in high walking frequency as a normal state again. At around 120s, we blocked one leg of MORF to which the DIL reacted by reducing φ to a very low value; thereby the walking frequency slowed down. If the leg became blocked for a longer period of time, the DIL would eventually decrease φ to almost zero. As a consequence, MORF will stop moving. This way, the DIL can protect the robot from damage. A video of the experiment can be found in the supplementary material (video SM4.mp4). It is important to note that even though a tripod gait is used in all experiments, the DIL can also be applied to other gaits including dynamic ones. This is because the DIL will adapt the CPG frequency to the maximum one at which the tracking error is low (cf. Fig. 9) (i.e., independent of the gait/motion being used). However, additional balancing or posture control for stability may be required for dynamic gaits.

E. Adaptation for a compliant robotic manipulator arm

The final experiment was designed to determine the generality of the DIL mechanism. In this experiment, the GummiArm robot was used to follow a sawing-like motion. The DIL parameters were set to one-half of the values used for the MORF hexapod robot (i.e., $A_f = 0.3$, $A_s = 0.45$, $B_f = 0.4$, $B_s = 0.2$, $C_f = 0.0075$, $C_s = 0.0025$, and a bias of 0.008). The reason for doing so was that the GummiArm produces greater tracking errors due to a larger range of motion and more compliant joints. Furthermore, it shows that the parameters of the DIL are not that sensitive and do not require fine tuning. After 40s when the DIL had initially adapted the CPG frequency, a person stepped in front of the arm and blocked its motion for a few seconds.

As shown in Fig. 13, the DIL mechanism can adapt the frequency initially to fit the GummiArm and quickly decrease it when the motion is blocked. This behavior can be seen as both a self-protection mechanism to prevent damage to the arm itself and a behavior to protect any workers around the robotic arm. A video of the experiment can be found in the supplementary material (video SM5.mp4). Note that the tracking error is noisier when compared to that of the MORF hexapod robot due to the high compliance of the system (Fig.

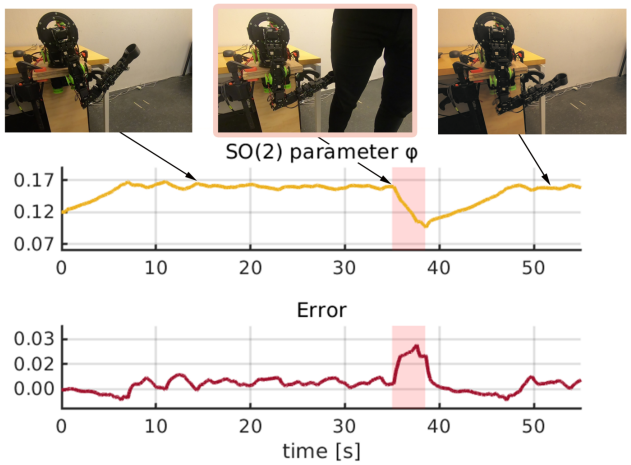

Fig. 13: Adaptation of φ to an external perturbation using the DIL. At 20s (red zone) the arm is blocked. The DIL immediately reduces φ in response to the high tracking error, resulting in slow arm movement. The arm and any person nearby is in this way protected from damage.

12) and that the adaptation is a bit slower due to the smaller learning parameters.

V. CONCLUSION

This letter demonstrates how we developed an error-based learning mechanism called DIL and applied it to neural CPG-based control of a hexapod robot called MORF. We showed that the DIL can be used to quickly reduce tracking error between actual and desired joint movements. It does so by adapting the CPG frequency to the highest level where the joint movements can follow the trajectory generated by the CPG-based control. In other words, the mechanism ensures that the CPG frequency matches and utilizes the performance of MORF. Besides adapting to the performance, the DIL is also able to adapt the frequency to a change in electrical power and unexpected external perturbations such as blocking a leg. When comparing the DIL with a state-of-the-art frequency adaptation mechanism (i.e., AFDC), it is clear that the DIL is both faster and better at reducing tracking error. This additionally results in more energy-efficient locomotion and straight walking even without steering control. The DIL uses parameters relating to error reduction, making it easier to tune for good performance. It is also important to emphasize that the DIL can achieve multiple adaptations (including adaptation to body property, damage protection, and unexpected energy drop) by relying only on a simple objective function (i.e., tracking error feedback) rather than multiple complex objective functions and robot kinematics. Furthermore, to illustrate the generality of the DIL mechanism, it was also successfully applied to control of a compliant robotic manipulator arm called GummiArm. Finally, it is important to note that mechanisms (like trajectory optimization) can also be added on top of the DIL mechanism to achieve amplitude or waveform adaptation.

In the future, we plan to investigate if the DIL parameters including the bias can relate to the CPG frequency and tracking error, in order to tune the DIL in a principled way. We also plan to investigate if the frequency adapted by the DIL is near the resonance frequency of the system. In order to do this we also need to examine the possibility of using DIL for force controlled systems. Finally, we plan to investigate if it is possible to extract the tracking error in different ways such that the DIL can be applied to arbitrary trajectories and does not have to rely on the waveform of the CPG output.

REFERENCES

[1] H. Yu, W. Guo, J. Deng, M. Li, and H. Cai, "A CPG-based locomotion control architecture for hexapod robot," in *Proc. of 2013 IEEE/RSJ Int. Conf. on Intelligent Robots and Systems*, Nov 2013, pp. 5615–5621.
[2] P. Ramdya, R. Thandiackal, R. Cherney, T. Asselborn, R. Benton, A. J. Ijspeert, and D. Floreano, "Climbing favours the tripod gait over alternative faster insect gaits," *Nat. Commun.*, vol. 8, pp. 1–11, 2017.
[3] L. Minati, M. Frasca, N. Yoshimura, and Y. Koike, "Versatile locomotion control of a hexapod robot using a hierarchical network of nonlinear oscillator circuits," *IEEE Access*, vol. 6, pp. 8042–8065, 2018.
[4] G. Zhong, L. Chen, Z. Jiao, J. Li, and H. Deng, "Locomotion control and gait planning of a novel hexapod robot using biomimetic neurons," *IEEE Trans. Control Syst. Technol.*, vol. 26, no. 2, pp. 624–636, Mar. 2018.
[5] A. Cully, J. Clune, D. Tarapore, and J.-B. Mouret, "Robots that can adapt like animals," *Nature*, vol. 521, p. 503, may 2015.
[6] S. Steingrube, M. Timme, F. Woergoetter, and P. Manoonpong, "Self-organized adaptation of a simple neural circuit enables complex robot behaviour," *Nat. Phys.*, vol. 6, no. 3, p. 16, 2011.
[7] A. Schneider, J. Paskarbeit, M. Schaeffersmann, and J. Schmitz, "HECTOR, a New Hexapod Robot Platform with Increased Mobility - Control Approach, Design and Communication," in *in Proc. of the 6th AMiRE Symp., AMiRE 2011*, Jan. 2012, pp. 249–264.
[8] H. Cruse, T. Kindermann, M. Schumm, J. Dean, and J. Schmitz, "Walknet - a biologically inspired network to control six-legged walking," *Neural Networks*, vol. 11, no. 7, pp. 1435 – 1447, 1998.
[9] D. Owaki, M. Goda, S. Miyazawa, and A. Ishiguro, "A minimal model describing hexapedal interlimb coordination: The tegotae-based approach," *Frontiers in Neurorobotics*, vol. 11, p. 29, 2017.
[10] M. A. Smith, A. Ghazizadeh, and R. Shadmehr, "Interacting adaptive processes with different timescales underlie short-term motor learning," *PLOS Biology*, vol. 4, no. 6, pp. 1035–1043, 5 2006.
[11] L. Righetti, J. Buchli, and A. J. Ijspeert, "Dynamic hebbian learning in adaptive frequency oscillators," *Physica D: Nonlinear Phenomena*, vol. 216, no. 2, pp. 269 – 281, 2006.
[12] T. Nachstedt, C. Tetzlaff, and P. Manoonpong, "Fast dynamical coupling enhances frequency adaptation of oscillators for robotic locomotion control," *Frontiers in Neurorobotics*, vol. 11, p. 14, 2017.
[13] T. Nachstedt, "Adaptive neural oscillator with synaptic plasticity for robot locomotion control," Master's thesis, University of Göttingen, Wilhelmsplatz 1 (Aula) 37073 Gttingen, Mar. 2013.
[14] D. M. Wolpert, J. Diedrichsen, and J. R. Flanagan, "Principles of sensorimotor learning," *Nat. Rev. Neurosci.*, vol. 12, pp. 739–751, oct 2011.
[15] M. Thor, J. C. Larsen, and P. Manoonpong, "MORF - Modular Robot Framework," in *Proc. of The 2nd Int. Youth Conf. of Bionic Engineering (IYCBE2018)*. Frontiers, Nov. 2018, pp. 21–23.
[16] F. Pasemann, M. Hild, and K. Zahedi, "SO(2)-Networks as Neural Oscillators," in *Proc. of Computational Methods in Neural Modeling*. Berlin, Heidelberg: Springer Berlin Heidelberg, 2003, pp. 144–151.
[17] B. van der Pol, "Lxxxviii. on relaxation-oscillations," *Lond.Edinb.Dubl.Phil.Mag.*, vol. 2, no. 11, pp. 978–992, 1926.
[18] J. Rayleigh, *The Theory of Sound*. Macmillan and co., 1894, vol. 1.
[19] S. S. Barikhan, F. Wörgötter, and P. Manoonpong, "Multiple Decoupled CPGs with Local Sensory Feedback for Adaptive Locomotion Behaviors of Bio-inspired Walking Robots," in *From Animals to Animats 13*. Springer International Publishing, 2014, pp. 65–75.
[20] M. F. Stoelen, F. Bonsignorio, and A. Cangelosi, "Co-exploring actuator antagonism and bio-inspired control in a printable robot arm," in *From Animals to Animats 14*. Springer International Publishing, 2016, pp. 244–255.